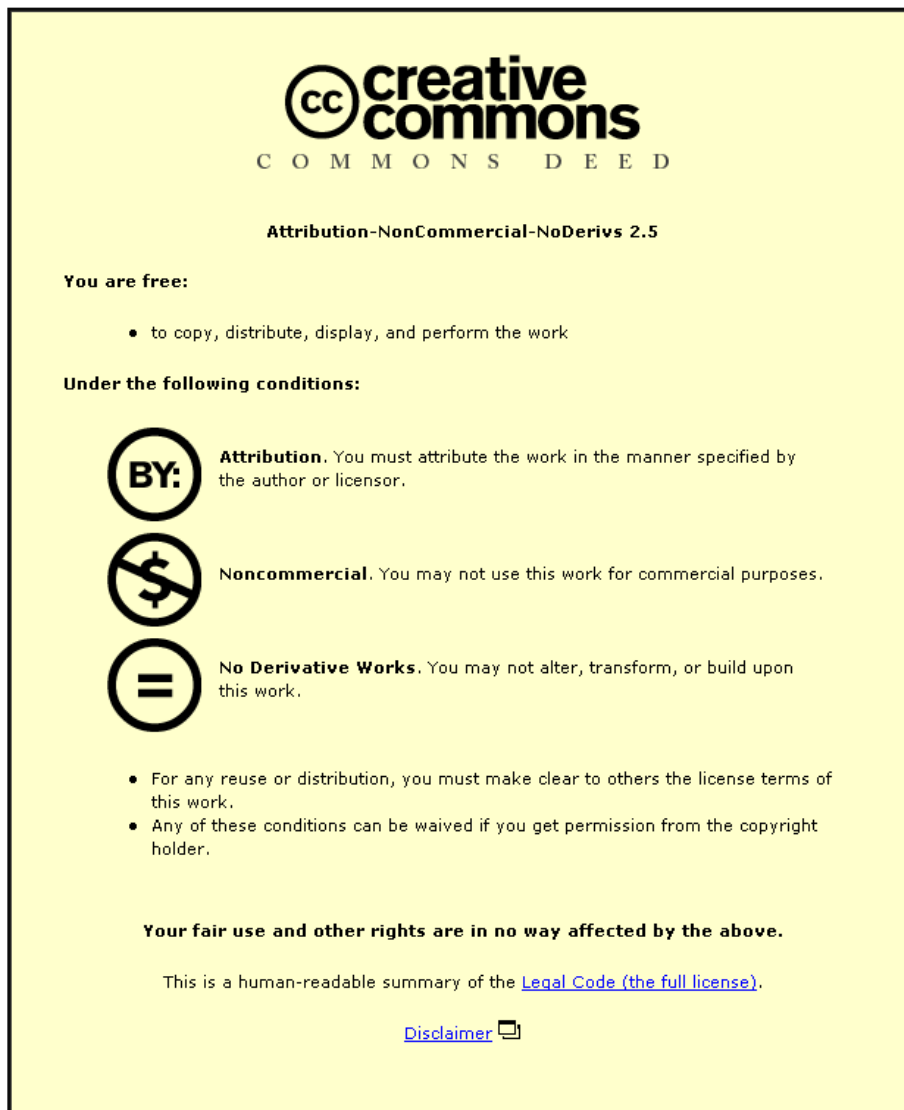




This item was submitted to Loughborough's Institutional Repository (<https://dspace.lboro.ac.uk/>) by the author and is made available under the following Creative Commons Licence conditions.



**CC creative commons**  
COMMONS DEED

**Attribution-NonCommercial-NoDerivs 2.5**

**You are free:**

- to copy, distribute, display, and perform the work

**Under the following conditions:**

**BY:** **Attribution.** You must attribute the work in the manner specified by the author or licensor.


**Noncommercial.** You may not use this work for commercial purposes.

**No Derivative Works.** You may not alter, transform, or build upon this work.

- For any reuse or distribution, you must make clear to others the license terms of this work.
- Any of these conditions can be waived if you get permission from the copyright holder.

**Your fair use and other rights are in no way affected by the above.**

This is a human-readable summary of the [Legal Code \(the full license\)](#).

[Disclaimer](#) 

For the full text of this licence, please go to:  
<http://creativecommons.org/licenses/by-nc-nd/2.5/>

## Effect of cylinder deactivation on the tribo-dynamics and acoustic emission of overlay big end bearings

M. Mohammadpour, R. Rahmani and H. Rahnejat<sup>§</sup>

Wolfson School of Mechanical & Manufacturing Engineering, Loughborough University,  
Loughborough, UK

<sup>§</sup>Corresponding author: [H.Rahnejat@lboro.ac.uk](mailto:H.Rahnejat@lboro.ac.uk)

### Abstract

The paper presents an integrated tribo-dynamics analysis of elliptic bore overlay big end bearings of internal combustion engines. The analysis focuses on bearing stability, frictional power loss and acoustic emission from these bearings, particularly with cylinder deactivation (CDA) with larger fluctuations in engine loading. The integrated approach represents a multi-physics analysis, not hitherto reported in literature, particularly under CDA. The analysis shows that CDA makes marginal differences in parasitic frictional losses in engine bearing performance and any significant gain would depend on the brake specific fuel consumption. It is also shown that sufficient swept volume with retained residual exhaust gas charge within the deactivated cylinders can ensure bearing whirl stability. Partially deactivated engine configurations exhibit a lower average steady noise emission, but with a higher degree of transient content. This suggests that there would be a greater contribution to engine rumble with deactivated cylinders.

**Keywords:** Elliptic bore big end bearings, bearing dynamics, thermo-mixed elastohydrodynamics, acoustic emission

### Nomenclature

$A$	Apparent contact area
$A_a$	Asperity contact area
$A_p$	Piston cross-sectional area
$A_v$	Area subject to viscous friction
$a, b$	Measures along the semi-major and semi-minor directions of elliptic bore
$C$	Centre of mass of the connecting rod
$c_{maj}$	Contact clearance along the semi-major axis
$c_{min}$	Contact clearance along the semi-minor axis

$c$	$c = \frac{c_{maj} + c_{min}}{2}$
$c_p$	Specific heat capacity
$d$	Shell (overlay) thickness
$E$	Young's modulus of elasticity
$E'$	Composite Young's modulus of elasticity of contacting solids $\left(\frac{1}{E'} = \frac{1-\nu_1^2}{E_1} + \frac{1-\nu_2^2}{E_2}\right)$
$e_0$	Eccentricity
$F_2, F_{5/2}$	Statistical functions
$F_{com}$	Combustion gas force
$F_{in}$	Inertial force
$f$	Total friction
$f_b$	Boundary friction
$f_v$	Viscous friction
$g$	Gravitational acceleration
$h$	Film thickness
$h_0$	Minimum film thickness
$h_i$	Coefficient of heat transfer
$i$	Contacting surface identifier ( $i = 1$ for bearing and $i = 2$ for journal)
$K$	Lubricant film stiffness
$k_l$	Thermal conductivity of lubricant
$k_s$	Thermal conductivity of solid

$L$	Bearing width
$l$	Connecting rod length
$\dot{m}$	Mass flow rate
$m_1$	Effective mass in translational motion
$m_{con}$	Equivalent translational mass of the connecting rod
$m_g$	Gudgeon pin mass
$m_p$	Piston mass
$n$	Iteration step
Nu	Nusselt number
$P_c$	Combustion gas pressure
$p$	Hydrodynamic pressure
$p_{in}$	Inlet lubricant supply pressure
$p_m$	Mean pressure
$p_{ref}$	Reference sound pressure
$p_{rms}$	Pressure fluctuations
$\dot{Q}$	Heat transfer (or generation) rate
$\dot{Q}_1$	Heat transfer rate to the bearing bushing
$\dot{Q}_2$	Heat transfer rate to the journal
$\dot{Q}_{cv}$	Convection heat transfer rate
$R_e$	Equivalent thermal barrier for convection due to mass flow
$R_f$	Thermal barrier due to surface flash temperature rise
$R_l$	Thermal barrier against heat conduction through lubricant film
$R_j$	Radius of the journal

$R_v$	Thermal barrier in the lubricant/solid surface interface (boundary layer)
$r$	Journal radius
$r_c$	Crank pin radius
$S_{fi}$	Characteristic lengths of conducting solids
$\bar{T}$	Time period
$T$	Temperature
$T_0$	Inlet temperature of the lubricant into the contact (also bulk housing temperature)
$T_e$	Effective (average) temperature of the lubricant
$T_f$	Friction induced torque
$T_p$	Applied combustion-induced power torque
$T_s$	Surface flash temperature
$t$	Time
$U$	Speed of lubricant entraining motion
$V$	Velocity of side-leakage flow along the bearing width
$W$	Contact reaction
$W_{con}$	Total weight of the connecting rod
$W_a$	Load carried by asperities
$W_h$	Hydrodynamic load carrying capacity
$x, y$	Lateral radial co-ordinates
$z$	Axial direction along the bearing width

#### **Greek symbols**

$\alpha$	Pressure viscosity of the lubricant
----------	-------------------------------------

$\beta$	Average asperity tip radius
$\beta_0$	Viscosity-temperature coefficient
$\gamma$	Slope of the lubricant limiting shear stress-pressure dependence
$\delta$	Local elastic deflection
$\Delta T$	Lubricant temperature rise
$\Delta T_{si}$	Surface temperature rise
$\varepsilon$	Eccentricity ratio
$\varepsilon_l$	Convergence criterion for load balance
$\theta$	Crank angle and circumferential direction in bearing
$\eta$	Lubricant dynamic viscosity
$\eta_0$	Lubricant dynamic viscosity at ambient conditions
$\lambda$	Stribeck's oil film parameter
$\lambda_{cr}$	Critical film ratio
$\nu$	Poisson's ratio
$\xi$	Asperity density per unit area
$\rho$	Lubricant density
$\sigma$	Composite RMS surface roughness ( $\sigma = \sqrt{\sigma_1^2 + \sigma_2^2}$ )
$\sigma_1$	Bearing surface roughness Ra
$\sigma_2$	Journal surface roughness Ra
$\tau$	Shear stress
$\tau_{L0}$	Limiting shear stress
$\phi$	Connecting obliquity angle
$\varphi$	Journal attitude angle

$\omega$  Angular speed of crank shaft (engine speed)

$\omega_0$  Natural frequency of lubricant film

### Abbreviations

BSFC Brake Specific Fuel Consumption

CDA Cylinder Deactivation

DOF Degrees of Freedom

IC Internal Combustion

NVH Noise, Vibration and Harshness

RMS Root Mean Square

SG Spheroidal Graphite

TDC Top Dead Centre

## 1- Introduction

Fuel efficiency, improved emissions and NVH (Noise, Vibration and Harshness) refinement are the key drivers in future power train development. Engine bearings play a key role in this quest. They are responsible for 20-30% of all parasitic frictional losses, which in turn account for 15-20% of all the engine losses [1]. Therefore, engine bearings represent 3-6% of the fuel energy expended in an IC (Internal Combustion) engine. This amounts to a significant proportion of all the power train energy consumption. Furthermore, engine bearings are subjected to progressively increased loading with the development trend of more compact high output power-to-weight ratio engines. This means that bearings operate at higher fluctuating loads with a greater variation in journal eccentricity. Thus, a greater chance of direct surface interaction exists at high eccentricity ratios which can culminate in wear.

Variable valve actuation (VVA) is a well-recognised method for reducing fuel consumption. Cylinder deactivation (CDA), discrete variable valve lift (DVVL) and continuously variable valve lift (CVVL) are different forms of VVA. In particular, CDA is seen as effective at low and partial engine loading conditions [2]. These conditions represent idling or low speed crawling in congested traffic, which progressively represent a greater proportion of everyday driving. CDA can also be applied at higher speeds with lower power requirement such as highway cruising. The obvious benefit of CDA is fuel economy as the result of reduced pumping losses. There are further benefits due to increased exhaust temperature under partial

loading, yielding improved after-treatment efficiency for diesel engines which helps the three-way catalyst technology [3,4].

As already noted, NVH refinement is also progressively a key design objective and regarded as a measure of vehicle quality. Engine order vibrations are the direct result of inertial imbalance and induced power torque which is a function of cylinder pressure [5]. When a cylinder is deactivated, usually all its intake and exhaust valves remain closed. This means that a volume of previously trapped air or the exhaust gas charge is retained within a deactivated cylinder. Therefore, cylinder-to-cylinder pressure variation, exacerbated by CDA can lead to engine order vibration that would have been otherwise removed with the full engine operation through suitable cylinder phasing and firing order [5]. Therefore, the use of CDA is somewhat limited by the NVH refinement because of the resulting greater fluctuations in the output power torque [2,6].

Development of light weight power train systems has been an ongoing trend for some time. This also improves fuel efficiency by reducing inertial imbalance, but can lead to a host of undesired phenomena. One is the increased elastodynamic response of lighter and compliant components. A plethora of power train NVH issues have emerged in recent times as the result of this trend, because of the broader NVH spectral composition [7-9]. Another potential problem is that the reduced inertial loading of engine bearings, particularly with deactivated cylinders, can increase the chance of engine bearings' whirl instability [10]. Therefore prediction of performance of engine bearings has become an even more important design issue than hitherto. The effect of fluctuating loads is more pronounced for the big endbearings which are directly affected by the combination of combustion and inertial loading [11]. To improve bearing stability, stiffness characteristics and load carrying capacity, these bearings are made in non-circular geometry (elliptic/lemon-shaped or multi-lobed), thus encouraging formation of multi-convergent wedges along the bearing periphery [11]. This action also reduces undue variations in the operating eccentricity, thus aiding bearing stability with increasing fluctuating loads in modern engines with a lower number of cylinders.

There are many interacting parameters in the design analysis of big end bearings. These include prediction of film thickness, contact pressure distribution and generated friction. There are also consideration of thermal effects as well as bearing stability and NVH issues. Various reported analyses have put emphasis on some of these considerations. The first important aspect to take into account is the dynamic nature of big end bearing response under fluctuating loads. Bates et al [12] presented an experimental investigation and a theoretical model for dynamically loaded big end bearings. They neglected the effect of any distortion or lubricant cavitation. Conway-Jones et al [13] presented a numerical model for thermal analysis of big end bearings. They included the effect of bearing distortion through inclusion of bearing shell flexibility using finite element method. Aitken et al [14, 15] investigated dynamically loaded big end bearings, assuming elastohydrodynamic contact conditions. These conditions usually occur with overlay bearings where several layers of soft (low elastic



modulus materials) are rolled upon the parent bearing bushing substrate in order to encourage localised deformation in the high pressure wedge region [10,16]. In fact, the pressures may be sufficient to deform the layers, but not usually of sufficient magnitude to induce piezo-viscous action of the lubricant. These conditions are often referred to as iso-viscous elastic or soft elastohydrodynamics [10]. A thin hard layer such as bismuth or indium is often coated on the overlay to resist wear of contacting surfaces when a thin film results, such as under start-up conditions or at low speeds [16]. Many analyses ignore the effect of overlay or the hard wear-resistant coating in the calculation of friction.

Other investigations of big end bearing dynamic response include the work of Boedo and Booker [17], who investigated film thickness and pressure distribution under dynamic oscillating conditions. Calculation of loading was based on a finite element deformation model. Bonneau et al [18] also presented a numerical procedure, based on Newton-Raphson iterations. They included the structural deformation in an elastohydrodynamic analysis with inclusion of lubricant cavitation. A multi-body dynamics approach, including the effect of soft overlay or thin shell construction, using the analytical column method approach for calculation of deformation was reported by Rahnejat [19] for a single cylinder engine for crankshaft circular bushing main support bearings under isothermal conditions. This approach was extended by Balakrishnan et al [16] for overlay crankshaft bearings, taking into account shear heating of the lubricant film. They included the effect of complex direct and moment loading with various cylinder firing in a compact 4-cylinder engine. It was shown that one repercussion of soft thermo-elastohydrodynamics with low loads was the adverse journal stability. Another repercussion was thin films under heavy loads, resulting in direct interaction of the surfaces.

Therefore, for all engine bearings the inclusion of thermal effects is an important prerequisite as well as the consideration of realistic rough boundary interactions. Mishra et al [11] reported such a model for big end bearings with varying bore order (out-of-roundness) and with different roughness patterns; longitudinal, transverse and isotropic forms using appropriate lubricant film expectancy functions. Majumdar [20] also carried out a comprehensive study of similar roughness patterns, showing an increase in the load carrying capacity of the bearing with a transverse roughness pattern, whilst the converse was found to be the case for a longitudinal pattern. He concluded that the control of manufacturing processes, particularly finishing operations on both the journal and bushing surfaces can enhance lubrication of big end bearings, particularly with respect to enhanced load capacity and reduced friction. Other representative literature dealing with thermo-elastohydrodynamic analysis of big end bearings include those of Kim et al [21], Stefani et al [22], Crosby [23] and Boncompain et al [24], who included the effect of heat conducted into the boundary solids; the journal and the bearing bushing. The surface temperature of the solids can then be used to study the structural integrity of surfaces, in particular any bushing overlay or coating.

Despite a large volume analyses of big end bearings, a combined study of bearing dynamics, lubrication and acoustics has not been reported particularly for modern trends in engine technology such as the effect of CDA on bearing performance. This paper presents a thermo-

mixed-elastohydrodynamic model for elliptic bore big endjournal bearings with application of CDA and its influence upon the key measures of performance; frictional power loss, fuel efficiency, dynamic stability and NVH refinement.

## 2- Theory

### 2.1- Applied loads

Big end bearings are subjected to transient applied loads as the result of varying in-cycle piston kinematics (thus inertial loading) and the combustion pressure. For a typical cylinder the inertial imbalance force along the axis of the piston is [5]:

$$F_{in} \approx m_1 r_c \omega^2 \left( \cos \omega t + \frac{r_c}{l} \cos 2\omega t \right) \quad (1)$$

where engine order vibrations up to the second engine order are considered for the 4-cylinder 4-stroke engine [5], and  $m_1$  is the equivalent mass in translation, which is that of the piston, the gudgeon pin and a proportion of the mass of the connecting rod in translation,  $m_{con}$ . This is obtained by assuming the single cylinder geometry as a two degrees of freedom system; one in translation and the other in rotation. Hence:  $m_1 = m_p + m_g + m_{con}$ , where [25]:

$$m_{con} = \frac{W_{con}}{g} \left( 1 - \frac{C}{l} \right) \quad (2)$$

where,  $W_{con}$  is the weight of the connecting rod.

The applied combustion force on the big end bearing is obtained in terms of the instantaneous connecting rod obliquity angle as [5]:

$$F_{com} = \frac{P_c A_p}{\cos \phi} \quad (3)$$

where:

$$\cos \phi \approx 1 - \frac{r_c^2}{2l^2} \sin^2 \omega t \quad (4)$$

Therefore, the total load applied on the bearing is expressed as:

$$F = \frac{F_{in}}{\cos \phi} + F_{com} \quad (5)$$

These are the forces transmitted to the bearing through the piston system. Any centrifugal force applied to the journal as the result of crank eccentric rotation is not taken into account in the analysis, except in the case of bearing stability chart. Therefore, the analysis assumes a balanced crankshaft.

This represents the maximum direct transient applied load which is carried by the big end bearing at any instant of time. There is also smaller moment loading contribution from adjacent cylinders, ignored in the current analysis. A detailed bearing loading analysis is provided by Balakrishnan et al [16]. Ideally, the applied load is carried by a lubricant film formed in the journal-bushing conjunction (i.e. the elastohydrodynamic reaction). However, a coherent film of lubricant is not always assured due to the transient nature of engine operations (load-speed combination as well as stop-start conditions). Hence, some of the applied load is carried by the direct contact of surfaces, usually a small portion of the rough topography of the crank-pin and the bushing surface (i.e. the asperity load). The latter is usually overlaid with a sandwich of soft and hard layers which also deform locally as the result of conjunctional pressures, conditions which are referred to as elastohydrodynamic. Therefore:

$$W = W_h + W_a = F \quad (6)$$

where, the elastohydrodynamic reaction is obtained as:

$$W_h = \int \int p(\theta, z) r d\theta dz \quad (7)$$

The asperity or boundary load is a function of surface roughness. For an assumed Gaussian distribution of asperities [26]:

$$W_a = \frac{16\sqrt{2}}{15} \pi (\xi\beta\sigma)^2 \sqrt{\frac{\sigma}{\beta}} E' A F_{5/2}(\lambda) \quad (8)$$

where, the statistical function  $F_{5/2}(\lambda)$  is a function of Stribeck oil film parameter  $\lambda = \frac{h}{\sigma}$ , where  $\sigma$  is the composite root mean square roughness of the contiguous surfaces. The statistical function can be represented by a polynomial-fit function as [27]:

$$F_{5/2}(\lambda) = \begin{cases} -0.004\lambda^5 + 0.057\lambda^4 - 0.296\lambda^3 + 0.784\lambda^2 - 1.078\lambda + 0.617; & \text{for } \lambda \leq \lambda_{cr} \\ 0 & ; \text{for } \lambda > \lambda_{cr} \end{cases} \quad (9)$$

where,  $\lambda_{cr} \simeq 3$  is the critical film ratio below which mixed regime of lubrication (including asperity interactions) occurs.

According to [26,28], the roughness parameter ( $\xi\beta\sigma$ ) is reasonably constant with a value in the range of 0.03 to 0.05 for steel surfaces. The ratio  $\sigma/\beta$  is a representation of the average asperity slope [10] and is in the range  $10^{-4}$  to  $10^{-2}$  according to Teodorescu et al [27]. In the current study it is assumed that  $\sigma_1 = \sigma_2$ ,  $\xi\beta\sigma = 0.055$  and  $\sigma/\beta = 0.001$ . Since a thin smooth hard layer of bismuth is applied as the outer layer of the shell overlay, the boundary friction is assumed to largely depend on the rougher surface of the steel crank pin.

## 2.2- Elastohydrodynamic conjunction

### 2.2.1- Generated lubricant pressures

In order to obtain the hydrodynamic load carrying capacity in equation (7) the generated instantaneous pressure distribution in the bearing should be obtained using Reynolds equation:

$$\frac{\partial}{\partial x} \left( \frac{h^3}{\eta} \frac{\partial p}{\partial x} \right) + \frac{\partial}{\partial z} \left( \frac{h^3}{\eta} \frac{\partial p}{\partial z} \right) = 6 \left( U \frac{\partial h}{\partial x} + V \frac{\partial h}{\partial z} + 2 \frac{\partial h}{\partial t} \right) \quad (10)$$

where:  $U = \frac{1}{2} \omega r$  is the speed of lubricant entraining motion into the bearing conjunction in circumferential direction  $x$  (viewed as unwrapped:  $x = r\theta$ ) and  $V$  is the velocity of any side-leakage flow along the bearing's length,  $z$  along the axis of the crank pin. The ultimate term on the right-hand side of the equation is lubricant entrapment in a dynamically converging gap, referred to as squeeze film motion. This retains the time history of lubricant film thickness under transient conditions. This term can be replaced in terms of crank dynamics as:

$$\frac{dh}{dt} = \frac{dh}{d\theta} \frac{d\theta}{dt} = \omega \frac{dh}{d\theta}$$

This substitution is made in Reynolds equation, resulting in a crank-angle based version of the equation which is more usual for engine bearing analysis.

Reynolds equation can be simplified using realistic assumptions. Firstly, the big end bearings generally used in modern vehicles are short-width bearings:  $\frac{2r}{L} > 2$ , where  $r$  is the journal radius and  $L$  is its length along the crank pin (often referred to as the bearing width). In such cases:  $\frac{\partial p}{\partial z} \gg \frac{\partial p}{\partial x}$ , thus  $\frac{\partial p}{\partial x} = 0$ . Secondly, a negligible side leakage flow along the bearing width is also assumed, thus:  $V = 0$ .

Implementing the above assumptions, Reynolds equation for a short-width engine bearing becomes:

$$\frac{\partial}{\partial z} \left( \frac{h^3}{\eta} \frac{\partial p}{\partial z} \right) = 6 \left( \omega \frac{\partial h}{\partial \theta} + 2 \frac{\partial h}{\partial t} \right) = 18\omega \frac{\partial h}{\partial \theta} \quad (11)$$

The conjunctional gap shape (i.e. film thickness,  $h$ ) and the variation of lubricant dynamic viscosity  $\eta$  are required for the solution of equation (11).

Equation (11) is the standard Reynolds equation for transient conditions. It does not take into account the effect of cavitation in the unloaded region of the bearing. Cavitation is an important phenomenon affecting erosion of bearing surfaces. This is not the focus of the paper. To include the effect of cavitation suitable boundary conditions at the contact exit must be employed. Interested readers can refer to Elrod's cavitation algorithm [29] as a modification to Reynolds equation.

### 2.2.2- Lubricant rheological state

The lubricant viscosity increases with pressure and reduces with temperature. Its rise with pressure is a function of the product  $\alpha p$  where  $\alpha$  is its piezo-viscosity coefficient, which is  $\alpha \approx 10^{-8} \text{ m}^2/\text{N}$  for most engine oils. Pressures in the conforming contact of engine bearings are usually of the order of a few to tens of MPa. Thus, the product  $\alpha p \ll 1$ , and the conditions are considered to be iso-viscous. Hence, in such cases one may confine the analysis to the variation of lubricant viscosity with temperature as [5]:

$$\eta = \eta_0 e^{-\beta_0 \Delta T} \quad (12)$$

where,  $\eta_0$  is the lubricant dynamic viscosity at a given temperature, such as the bulk temperature at the bearing housing,  $T_0$ , and  $\beta_0$  is the viscosity-temperature coefficient.  $\Delta T = T - T_0$ , is the rise in lubricant temperature from that in bulk.

### 2.2.3- Conjunctional film shape

Referring to figure 2, for an elliptic-bore journal bearing the film thickness  $h$  is obtained as:

$$h(\theta) = \frac{ab}{\sqrt{a^2 \sin^2 \theta + b^2 \cos^2 \theta}} - r - x \cos \theta - y \sin \theta + \delta \quad (13)$$

where,  $0 \leq \theta \leq 2\pi$ ,  $a = r + c_{min}$  and  $b = r + c_{maj}$  (Figure 1).

where  $x$  and  $y$  are the lateral excursions of journal centre from the geometric centre of the bearing bushing (radial eccentricities) at any instant of time:

$$x = e_0 \sin \varphi \text{ and } y = -e_0 \cos \varphi \quad (14)$$

where  $e_0$  is the eccentricity and  $\varphi$  is the journal attitude angle relative to the vertical radial direction (Figure 1).

The term  $\delta$  in equation (13) represents the deflection of the soft bearing bushing overlay. The conforming nature of journal-bushing contact and the low elastic overlay, such as Babbitt (A Tin based alloy) or copper means that local deflection of the bushing surface at any given location may be considered to be almost entirely due to an assumed column of local pressure directly orthogonal to it. Using the tri-axial state of stress-strain for a compressible shell material subjected to internal pressure and noting that for plane strain contact mechanics problems the compressive contact stress equates the localised pressure (i.e. the column method), Rahnejat [19] showed that:

$$\delta = \frac{(1-2\nu)(1+\nu)d}{E(1-\nu)} p \quad (15)$$

where  $d$  is the shell thickness (in this case the thickness of the soft Babbitt layer of the bushing overlay) and  $E$  and  $\nu$  are the Young's modulus of elasticity and Poisson ratio of the layer.

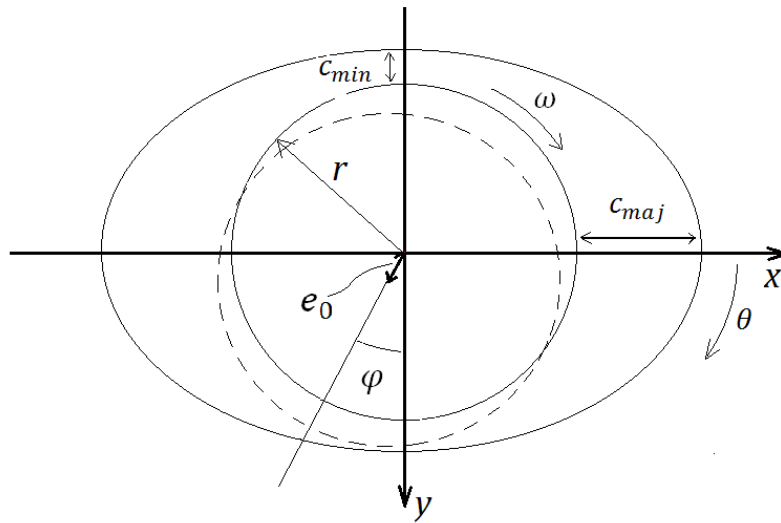


**Figure 1: Elliptic bearing configuration**

A time-efficient analytical–numerical approach can be used to obtain the pressure distribution required for equation (7). Reynolds equation (11) is integrated twice with respect to the coordinate  $z$ , employing the boundary conditions:  $p(\theta, 0) = p(\theta, L) = 0$ . This leads to:

$$p(\theta, z) = \frac{9\eta z(z-L)}{h^3} \omega \frac{\partial h}{\partial \theta} \quad (16)$$

where, using equation (13):

$$\frac{\partial h}{\partial \theta} = \frac{-ab(a^2-b^2) \sin \theta \cos \theta}{(a^2 \sin^2 \theta + b^2 \cos^2 \theta)^{3/2}} + x \sin \theta - y \cos \theta + \frac{d\delta}{d\theta} \quad (17)$$

A simultaneous solution of equations (12), (13), (15) and (16) is required, with the unknowns  $p$ ,  $h$ ,  $\delta$ ,  $\eta$  and  $\Delta T$ . Therefore, an isothermal solution ( $\Delta T = 0$ ) can readily be obtained for  $\eta = \eta_0$ . However, temperature plays a significant role as it affects the lubricant viscosity, thus the lubricant film thickness and its load carrying capacity.

#### 2.2.4- Thermal analysis

An analytical method based on a control volume approach described in Morris et al [30] is used in the current study to calculate the average temperature rise for the lubricant passage through the contact as well as the rise in the temperatures of the bounding surfaces; the journal and the bearing bushing.

Within the contact, the rate of heat generation through viscous shear of a film of lubricant is:

$$\dot{Q} = \omega T_f \quad (18)$$

where  $T_f$  is the viscous friction torque:

$$T_f = \int_0^{2\pi} \int_0^L \tau r d\theta dz \quad (19)$$

Part of the generated heat in the contact is dissipated through the bearing bushing,  $\dot{Q}_1$  and the journal,  $\dot{Q}_2$ . The remainder is carried away by the lubricant through convection,  $\dot{Q}_{cv}$ . Hence (Figure 2, the abscissa represents the bearing periphery):

$$\dot{Q} = \dot{Q}_1 + \dot{Q}_2 + \dot{Q}_{cv} \quad (20)$$

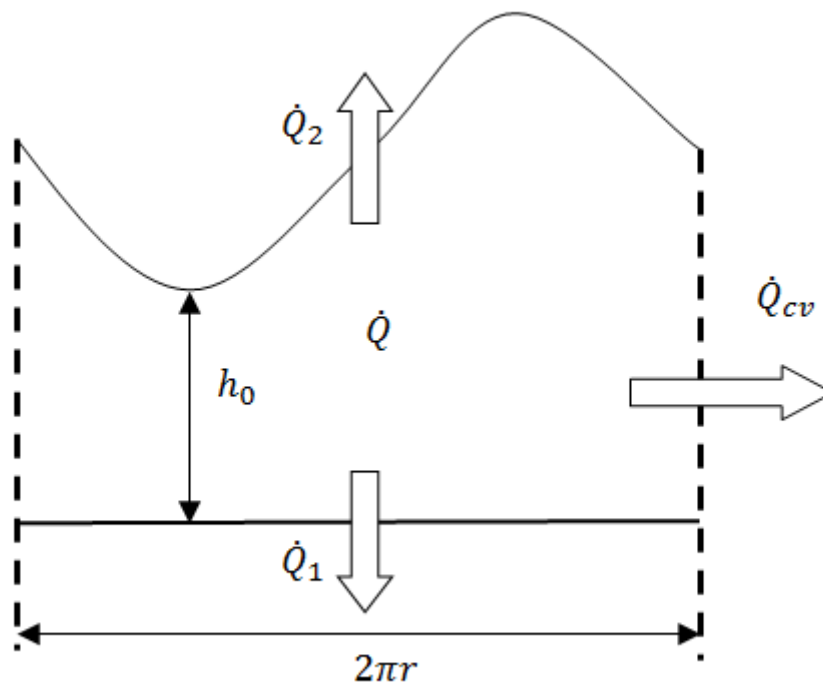


**Figure 2: Thermal flow through the contact**

Any heat conducted through small asperity pair contact interfaces is neglected as the asperity contact area typically constitutes less than 1% of the total contact area [26, 27].

The heat removal rate due to lubricant mass flow in the contact is readily obtained (Figure 3):

$$\dot{Q}_{cv} = \frac{T_e - T_0}{R_e} = \frac{\Delta T}{R_e} \quad (21)$$

where,  $R_e = 1/(\dot{m}c_p)$  is the equivalent thermal barrier for the mass flow convection,  $T_0$  is the inlet contact temperature of the lubricant,  $T_e$  is the effective (average) temperature of the

lubricant in the contact and  $c_p$  is the specific heat capacity of the lubricant at constant pressure. The mass flow rate is obtained as [10,31]:

$$\dot{m} = 2\pi r \omega L c e_0 \rho + \frac{2\pi p_{in} r c^3 (1 + 1.5(e_0/c)^2)}{3\eta L} \quad (22)$$

where:  $c = \frac{c_{min} + c_{maj}}{2}$

By assuming that the heat generated is at the mid-depth of the lubricant film, then the heat flow to the bounding surfaces has to overcome a number of thermal resistive barriers (see Figure 3) [30]. These are the resistances due to the lubricant film thickness,  $R_l$ , the convective heat transfer through the boundary layer,  $R_v$  and a rise in the solid surface flash temperature,  $R_f$ . These resistance values are calculated through the following relationships [30]:

$$R_l = \frac{h_0}{2k_l A}, \quad R_v = \frac{1}{h_t A}, \quad R_f = \frac{S_f}{k_s A} \quad (23)$$

where,  $h_t$  is the heat transfer coefficient of the thin boundary layer and  $k_l$  and  $k_s$  are thermal conductivity of the lubricant and the solid surfaces respectively. In addition,  $h_0/2$  is considered as the characteristic length, where  $h_0$  is the minimum lubricant film thickness (Figure 2).

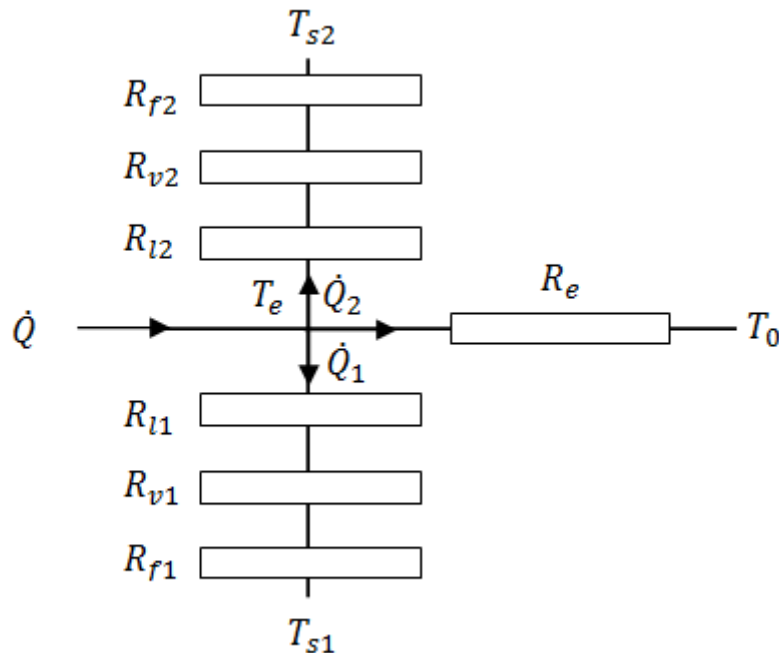


**Figure 3: Heat transfer within the contact**

The heat transfer coefficient,  $h_t$ , is obtained from the following relationship [32]:



$$h_t = \text{Nu} \frac{k_l}{h_0} \quad (24)$$

To calculate the Nusselt number, the laminar flow of lubricant through the conjunction is considered to be analogous to fluid flow through two infinite parallel surfaces with fully developed velocity and temperature profiles. This assumption is justified because the variation of temperature through the depth of the thin film is negligible. According to Suryanarayana [32] the Nusselt number for such a case is constant and for the current analysis has a value of  $\text{Nu} = 8.24$ .

The journal and bearing surfaces are always in contact with the heat source (i.e. the lubricant). Therefore, when the bearing is viewed as unwrapped, it can be assumed that the journal and bearing *rectangular* contact patch surface areas are supplied with a steady source of heat flow. As a result, the characteristic length for the bearing ( $i = 1$ ) and for the journal ( $i = 2$ ),  $S_{fi}$ , would be [33]:

$$S_{fi} = \frac{1}{2A} \left\{ (2\pi r)L^2 \sinh^{-1} \left( \frac{2\pi r}{L} \right) + L(2\pi r)^2 \sinh^{-1} \left( \frac{L}{2\pi r} \right) + \frac{1}{3} [L^3 + (2\pi r)^3 - (L^2 + (2\pi r)^2)^{1.5}] \right\} \quad (25)$$

The effective temperature is obtained as [30]:

$$T_e = \frac{(\dot{Q}_{Re} + T_0) \prod_{i=1}^2 R_i + R_e \sum_{i=1}^2 R_i T_{si}}{\prod_{i=1}^2 R_i + R_e \sum_{i=1}^2 R_i}, \quad i \in \{1,2\} \text{ and } i \neq j \quad (26)$$

Once the effective (average) lubricant temperature in the contact is found one can determine the effective viscosity of the lubricant using equation (12). Using a heat partitioning method described in [30], the temperature rise in the solid surfaces can be calculated, based on the quantity of transferred heat to them as:

$$\Delta T_{si} = \frac{R_{fi}}{R_i} (T_e - T_{si}), \quad i \in \{1,2\} \quad (27)$$

### 2.2.5- Friction in mixed regime of lubrication

As already noted in the Introduction one key aim of any analysis of engine bearings is prediction of frictional power loss. In bearings friction is mainly generated due to viscous shear of a lubricant film entrained into the contact. Additionally, if when the thickness of lubricant film is insufficient to completely separate the contacting surfaces, friction is also generated by interaction of rough features on the contiguous surfaces (boundary friction). Therefore, in mixed/boundary regime of lubrication, the friction at the tip of asperities must be taken into account. A very thin film of lubricant is usually adsorbed to the tip of surface asperities because of boundary active molecular species in engine lubricants. These boundary adsorbed films are subject to fairly high shear rate because of their very thin nature and the short contact transit time (i.e. high effective sliding velocity). Therefore, boundary friction comprises non-Newtonian shear of such thin films (first term in equation (28)), as well as

adhesive elasto-plastic friction of opposing asperities (second term in equation (28)) [34]. Thus, according to the very basic model proposed in [26]:

$$f_b = \tau_{L0}A_a + \gamma W_a \quad (28)$$

where,  $\gamma$  is analogous to the adhesive coefficient of friction at asperity level junctions and  $\tau_{L0}$  is the lubricant limiting shear stress [35], share of the contact load carried by the asperities,  $W_a$  is given by equation (8) and the total asperity contact area for an assumed Gaussian distribution of them is obtained as [26]:

$$A_a = \pi^2 (\xi\beta\sigma)^2 AF_2(\lambda) \quad (29)$$

The statistical function  $F_2(\lambda)$  is expressed as [27, 28]:

$$F_2(\lambda) = \begin{cases} -0.002\lambda^5 + 0.028\lambda^4 - 0.173\lambda^3 + 0.526\lambda^2 - 0.804\lambda + 0.500; & \text{for } \lambda \leq \lambda_{cr} \\ 0 & ; \text{for } \lambda > \lambda_{cr} \end{cases} \quad (30)$$

The contribution to friction from viscous shear of the uninterrupted (full) film of lubricant in the bulk of the contact,  $A_v = A - A_a$  with  $A_v \gg A_a$  is obtained as:

$$f_v = \int \left[ \pm h \frac{dp}{dz} + \frac{\eta}{h} U \right] dA_v \quad (31)$$

However, thin lubricant films may be subject to shear which exceeds the limiting shear stress:  $\tau > \tau_{L0}$ , in which case [26]:

$$f_v = \int (\tau_{L0} + \gamma p^*) dA_v \quad (32)$$

where  $p^* = \frac{W_h}{A_v}$

Therefore, the total friction becomes:

$$f = f_v + f_b \quad (33)$$

The frictional power loss for is obtained as:

$$P_l = fU \quad (34)$$

### 2.3- Acoustic emissions model

The most important aspect of NVH with regard to engine bearings is the noise radiated from them. This contributes to the overall engine noise output and its attenuation is progressively regarded as a refinement issue. The main source of noise is from air pressure fluctuations about a steady mean pressure value. These occur as the result of fluctuating bearing load due

to changes in combustion loading and inertial dynamics. The pressure fluctuations are represented by their root mean square value,  $p_{rms}$  for any given period of time  $\bar{T}$  [36]:

$$p_{rms} = \sqrt{\frac{1}{\bar{T}} \int_t^{t+\bar{T}} [p(t) - p_m]^2 dt} \quad (35)$$

where,  $p$  is the hydrodynamic pressure at any instant of time and  $p_m$  is the mean pressure at the steady state response period  $\bar{T}$ , which can be obtained as [36]:

$$p_m = \frac{1}{\bar{T}} \int_t^{t+\bar{T}} p(t) dt \quad (36)$$

The sound pressure level as the results of pressure perturbations can now be found as:

$$N = 20 \log \left( p_{rms} / p_{ref} \right) \quad (37)$$

where,  $p_{ref}$  is the reference sound pressure in the lubricant, taken as  $10^{-6}$  Pa [36].

#### 2.4- Bearing stability calculations

A critical issue with respect to engine bearings is their dynamic stability. Instability may be caused by a plethora of reasons, including loss of lubricant reaction or severe cases of fluctuating bearing load, termed as oil whirl condition [10]. Thin lubricant film thickness can also lead to significant direct contact of journal and its bushing, causing dynamic instability, known as dry whip [11]. Other effects such as edge loading of the contact as the result of misalignment or structural flexibility of the bearing can also lead to instability [17]. The lubricant film under the simulated conditions of the current analysis is of sufficient thickness to guard against instability caused by dry whip. Furthermore, the current analysis does not take into account any journal misalignment. Figure 4 shows a stability chart with the locus line  $\omega_0/\omega$  confining the region where unstable oil whirl can occur due to lack of journal bearing load (reduced inertia) or increased journal speed [10]. The underlying analysis in creating of the stability chart is based on the speed ratio  $\omega_0/\omega$ , where  $\omega$  is the journal speed and  $\omega_0$  is the natural frequency of the lubricant film, when the lubricant film is considered as a spring and the journal-lubricant film as a single degree of freedom system, thus [10]:

$$f_0 = \frac{\omega_0}{2\pi} = \frac{1}{2\pi} \sqrt{\frac{gK}{W_h}} \quad (38)$$

where, the lubricant film stiffness non-linearity is obtained at any instant of time (crank angle) as:  $K = \frac{\partial W_h}{\partial h}$  and  $W_h$  is given by equation (7).

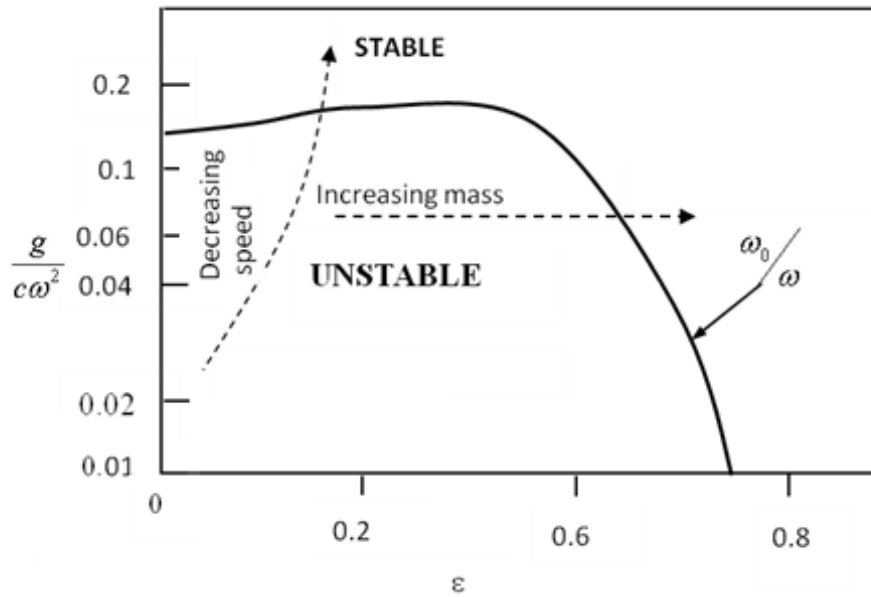


**Figure 4: Bearing Stability Chart (Gohar and Rahnejat [10])**

The stability chart shows the stable region of operation is usually for eccentricity ratios  $\varepsilon = e_0/c > 0.7$  for a broad range of engine speeds. The ordinate to the figure is termed the stability factor;  $\frac{g}{c\omega^2}$  which is a function of engine speed. In the current analysis the chart is used to ensure that the results presented fall within the stable region of the chart.

### 3. Method of Solution

The following step-wise iterative computational procedure is used:

Step 1: For a given engine speed  $\omega$  and a given crank angle  $\theta$ , the connecting rod angle  $\varphi$  is calculated from equation (4) and the applied bearing load from equation (5).

Step 2: An initial value for eccentricity,  $e_0$  is assumed and the pressure distribution is calculated from Reynolds equation.

Step 3: The lubricant viscosity and film thickness are calculated from equations (12) and (13), the latter with an initial assumed value of  $\delta = 0$ .

Step 4: The applied pressures alter and cause deflection,  $\delta$  (equation (15)), which in turn changes the lubricant film thickness using equation (13). Consequently, the pressure distribution from Reynolds equation is altered. Also, changes in film thickness alter the value of  $\lambda$ , thus the statistical functions  $F_2(\lambda)$  and  $F_{5/2}(\lambda)$ . Furthermore, viscous and boundary friction contributions alter accordingly (equations (28) and (31)), which change the friction torque and the generated heat (equations (18) and (19)). The control volume thermal balance, described in section 2.2.4 result in an updated lubricant temperature,  $T_e$ , thus its rise,  $\Delta T$

from the initially assumed bulk temperature. This leads to change of lubricant viscosity, thus, lubricant film thickness, pressure distribution and other system variables. These changes alter the calculated values of  $W_a$  and  $W_h$ , hence the total reaction force,  $W$  in equation (6).

Step 5: Equation (6) constitutes an instantaneous quasi-static equilibrium (a constraint function), which is regarded as a convergence criterion as:

$$\epsilon_l = \frac{|F-W|}{F} < 0.01 \quad (39)$$

where,  $\epsilon_l$  is the limit of convergence.

Step 6: If the above criterion is not satisfied, then the initial assumed eccentricity is altered and the entire procedure from step 2 is repeated. Otherwise, the crank angle,  $\theta$  is advanced and simulated work continues for the entire engine cycle ( $0^\circ \leq \theta \leq 720^\circ$  for a 4 stroke engine).

During this procedure oil whirl stability and acoustic emission are ascertained after each crank angle converged conditions.

#### 4. Results and Discussion

The analysis carried out here corresponds to a c-segment 4-cylinder 4-stroke diesel engine under low speed (25 km/h) city driving condition at 25% throttle in second gear (ratio: 1:2.038) with the differential ratio of 1:4.07. For this condition the engine speed is 2200 rpm. Tables 1-3 provide all the necessary data used in the analysis. The results are presented for a cylinder subjected to deactivation as well as an active cylinder. Figure 5 shows the combustion load  $F_c$  and the calculated inertial force  $F_{in}$  along the connecting rod. The results correspond to the cases: (i)- all active cylinders, (ii)- an active cylinder in partially deactivated engine configuration and (iii)- a deactivated cylinder. The results also include the inertial unbalance force (purely reciprocating force) for any cylinder. It can be seen that a considerable increase in gas force is required in active cylinders (when some cylinder are deactivated) in order to maintain the same steady engine speed as that of the full engine operation. This means that a higher fuel injection rate is maintained which may not necessarily lead to improved fuel efficiency and reduced emissions with cylinder deactivation. However, the pumping losses would be reduced at lower injection rate. The current analysis does not deal with the pumping losses. The results also show the much reduced inertial force following the modern light weight power train philosophy. Combustion occurs at  $20^\circ$  past the TDC. The crank angle  $\theta = 0^\circ$  and every  $720^\circ$  thereafter mark the beginning of the power stroke in the figure. Note that combustion occurs later in active cylinders when some are deactivated. The maximum chamber pressure occurs immediately after the TDC in deactivated cylinders. The pressure in the deactivated cylinder is as the result of the swept volume of entrapped air and residual charge.

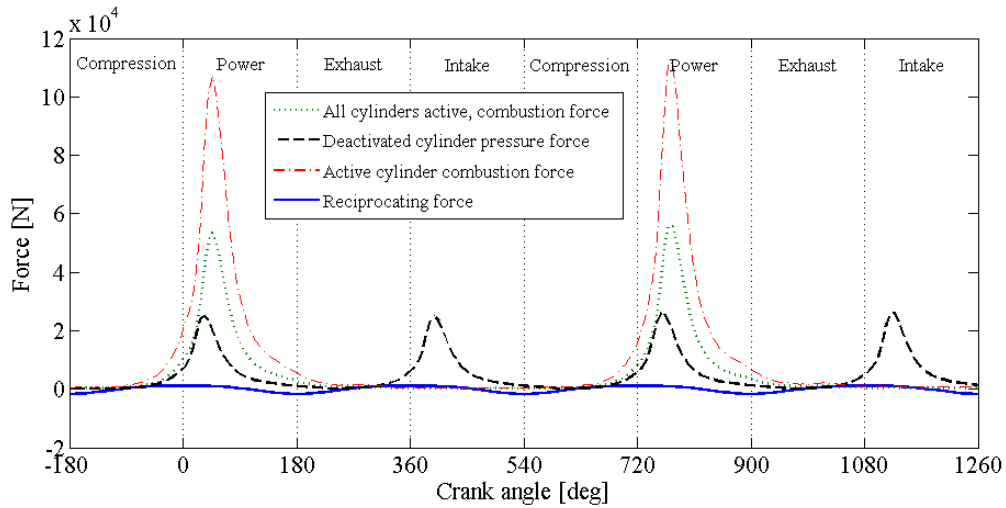


**Figure 5: Applied forces on bearing along the connecting rod**

**Table 1: Engine data**

Parameter	Value
Crank pin radius [mm]	31.0
Connecting rod length [mm]	107.0
Effective translational mass [g]	320.0
Engine speed [rpm]	712.0

**Table 2: Bearing data**

Parameter	Value
Bearing width [mm]	16.8
Bearing radius [mm]	21.0
Minor diametral clearance [ $\mu\text{m}$ ]	20.0
Major diametral clearance [ $\mu\text{m}$ ]	30.0
Composite surface roughness [ $\mu\text{m}$ ]	1
Shell thickness value [mm]	2.6

**Table 3: Lubricant and material data**

Parameter	Value
Lubricant dynamic viscosity [mPa.s]	8.0
Lubricant density [ $\text{Kg m}^{-3}$ ]	833.8
Viscosity-temperature coefficient [ $\text{K}^{-1}$ ]	0.026
Pressure-induced shear coefficient ( $\gamma$ )	0.047
Atmospheric limiting shear stress [MPa]	2.3
Specific heat capacity of lubricant [ $\text{J kg}^{-1} \text{K}^{-1}$ ]	2360
Thermal conductivity of lubricant [ $\text{W m}^{-1} \text{K}^{-1}$ ]	0.225
Poison's ratio for Babbitt [-]	0.33

Young's modulus for Babbitt [GPa]	60
Thermal conductivity of bearing bushing $k_{s1}$ [ $\text{Wm}^{-1}\text{K}^{-1}$ ]	46
Thermal conductivity of journal $k_{s2}$ [ $\text{Wm}^{-1}\text{K}^{-1}$ ]	25.96
Bulk oil temperature [ $^{\circ}\text{C}$ ]	80
Journal material	SG cast iron
Bearing overlay	Babbitt
Eyring shear stress [MPa]	5
Inlet pressure [MPa]	0.5

Figure 6 (a) shows the minimum film thickness in the big end bearing during the various engine cycles. In all the studied cases, the film thickness is reduced during piston reversals at the TDC ( $\theta = 0^{\circ}, 360^{\circ}, 720^{\circ}, \dots$ ) and attains its minimum value in the power stroke ( $\theta = 0^{\circ}, 720^{\circ}, \dots$ ). In fact, a mixed regime of lubrication ( $1 \leq \lambda \leq 4$ ) is noted in all the cases as indicated by the demarcation boundaries in the figure. Therefore, the inclusion of boundary friction is quite important in the prediction of frictional power loss.

As the result of a thinner film in active cylinders of a partially deactivated engine cylinders, the big end bearings of these cylinders exhibit larger frictional losses (figure 6(b)). The deactivated cylinders have reduced frictional power loss than any cylinders in the normal engine operation. However, the cyclic power loss is spread over all the engine strokes rather than being confined mostly to the power stroke for active cylinders. Altogether, for a multi-cylinder engine with some deactivated cylinders, the results indicate that frictional power loss is not necessarily reduced under the prescribed conditions. One of the underlying reasons for this is the higher operating lubricant temperature in the bearings is the active cylinders of a partially deactivated engine configuration (figure 6(c)) as well as still significant generated temperatures in bearings of deactivated cylinders. Thus, the expected gain on fuel efficiency is not necessarily assured by cylinder deactivation based on engine bearings alone, unless provisions are made in fuel injection rate or running the engine at a lower rpm. It should be noted that with CDA there would be significant temperature rise in piston-cylinder system, which in turn would affect the bulk temperature distribution of the engine. These global effects through heat transfer are not taken into account in the current analysis, which is confined to local generated heat in the bearing conjunction itself.

For better comparison between CDA and the normal engine operation mode, the bearings' power loss can be presented in terms of the equivalent fuel consumed through parasitic loss (energy lost). The energy lost in a bearing can be obtained by integrating the power loss (Fig. 6(b)) with respect to time. Then, the average value can be obtained by dividing the same over the number of engine cycles. To obtain the equivalent fuel, the calculated energy is divided by the fuel's specific energy. The BSFC (brake specific fuel consumption) is typically 500 g/kWh for a C-segment vehicle engine in its normal operation mode and 350 g/kWh with CDA. The equivalent total fuel consumption for these two modes is presented in table 4. The lost fuel by all bearings is also provided in the table. Results show that despite a reduction in general fuel consumption with CDA (lower parasitic losses in piston conjunctions and valve train), the parasitic fuel loss in bearings is actually increased under the CDA mode. This

disadvantage is even worse when considering better BSFC under CDA. Therefore, there is a greater percentage parasitic fuel consumption in bearings with CDA.

**Table 4: Fuel consumption characteristics**

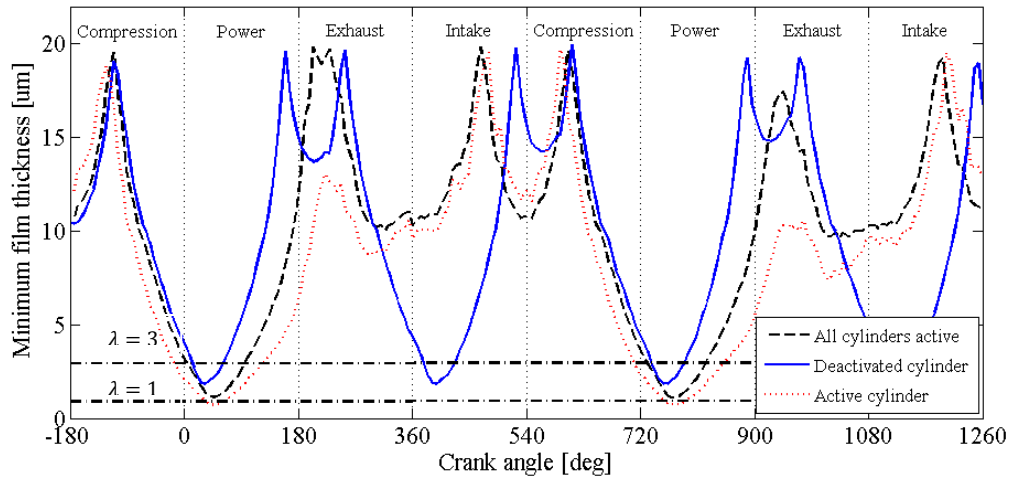
	BSFC [g/kWh]	Fuel consumption [g/s]	Bearing equivalent parasitic fuel loss [g/s]
All cylinders active	500	2.08	0.0031
CDA	350	1.46	0.0038

As already described in section 2.4 an important consideration in big end bearing design is its whirl stability under the breadth of engine operating conditions (load-speed combination at all operating temperatures). Therefore, for all such conditions there is a co-ordinate location in the stability chart of figure 4 as a function:  $f\left(\varepsilon, \frac{g}{c\omega^2}\right)$ . The eccentricity ratio;  $\varepsilon = e_0/c$  is a function of system dynamics (equation (14)), which is in turn a function generated contact pressures and hence the bearing load [10]. Therefore, with CDA the fluctuation in applied load can cause bearing instability with lower values of  $\varepsilon$ .

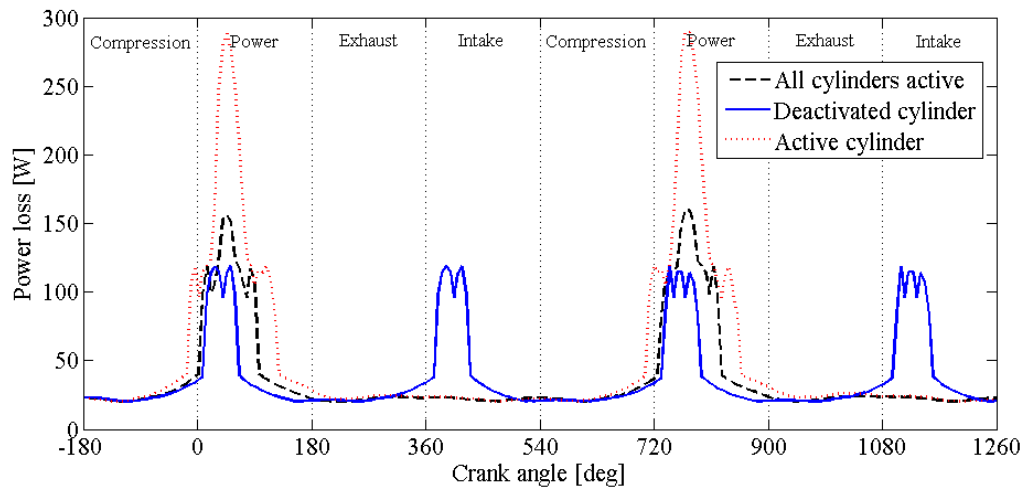
Figure 6(d) illustrates the variation in the value of stability factor. The minimum value of stability factor is 1.086 and is marked by the letter A in the figure. A comparison of this minimum stability factor value with those in the stability chart of figure 4 shows that the investigated conditions render stable dynamics throughout the engine cycle (residing well above the demarcation boundary line  $\omega/\omega_0$  for all the various cylinder conditions including for lightly loaded CDA with low values of  $\varepsilon$ ).

Fluctuating loads because of variations in combustion pressure (figure 5) result in corresponding variations in generated hydrodynamic pressures within the bearing. At any instant of time (any point on the graphs of figure 5), the integrated pressure distribution is the lubricant reaction which equates the applied force onto the bearing (see the convergence criterion (39)). These pressure perturbations contribute to noise emission. With CDA a larger variation in pressure perturbations is expected as the conjunctional film thickness is subjected to greater cyclic changes (figure 6(a)). Therefore, from an NVH refinement viewpoint it is essential to ascertain the implications of acoustic emission as described in section 2.3.

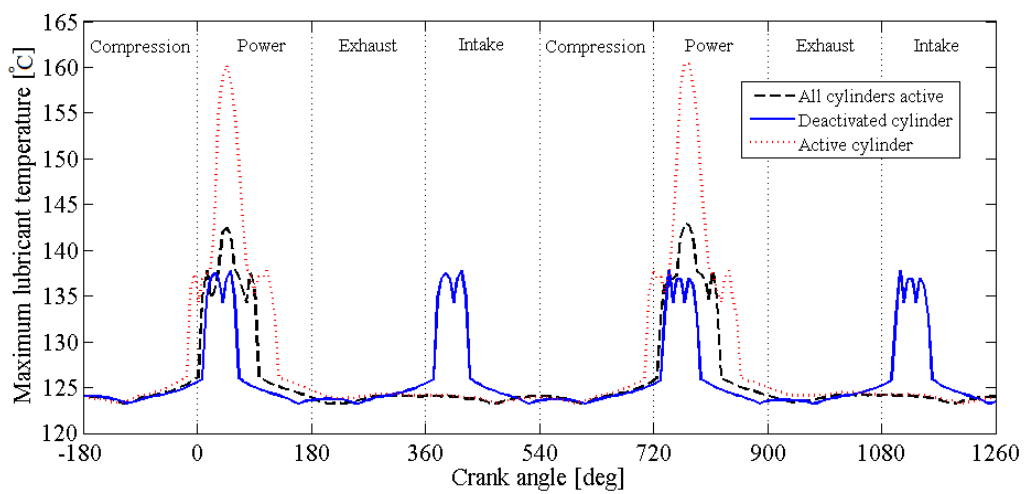




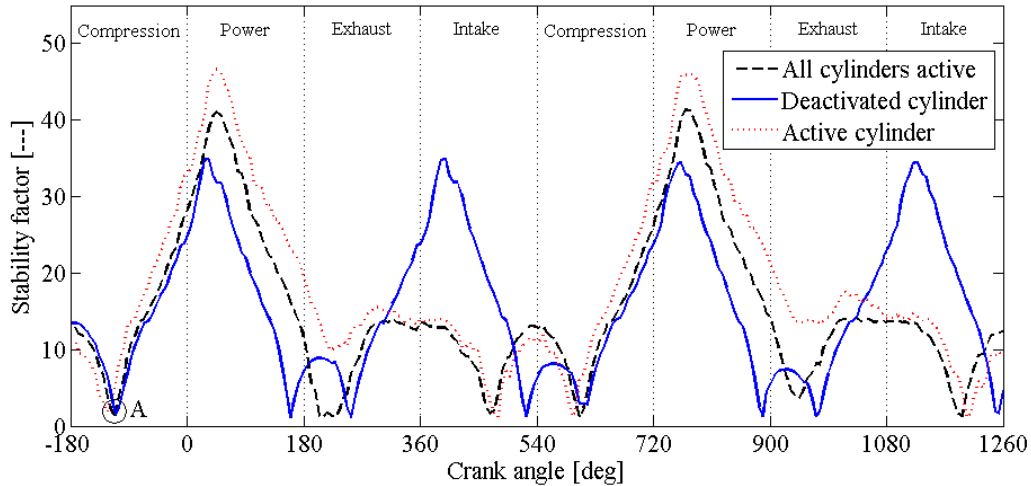
(a)



(b)



(c)



(d)

**Figure 6: General characteristic responses for various cylinder conditions (a): minimum film thickness, (b): power loss, (c): maximum lubricant temperature and (d): stability factor**

Figure 7 shows the sound pressure level big end bearings of the engine under normal operation. This indicates a steady average sound pressure level of around 92 dB, with superimposed perturbations of around 15 dB. The small sound pressure perturbations follow the spectral signature of the 4-stroke combustion process. These follow the power torque as a function of  $T_p \propto e^{ik\omega/2}$  with  $k$  being the harmonic number,  $i = \sqrt{-1}$  the complex number exponent and  $\omega$  the engine speed [5]. Therefore, at the speed of 2200 rpm, the fundamental combustion frequency is  $\omega/2 \approx 18.5$  Hz with its higher harmonics at  $k = 2, 3, 4, \dots$ . These contributions are evident in the sound pressure fluctuations. The low frequency low amplitude sound pressure variation contributes to engine rumble, which is a humming type response. Some people are quite sensitive to this transient noise response [37]. With CDA a higher variation in pressure perturbations is expected as the conjunctional film thickness is subjected to greater cyclic changes (figure 6(a)). The results tabulated in table 5 confirm this. They show that under CDA the maximum sound pressure level is higher. However, the average sound pressure level is lower than that of an engine under normal operation mode.

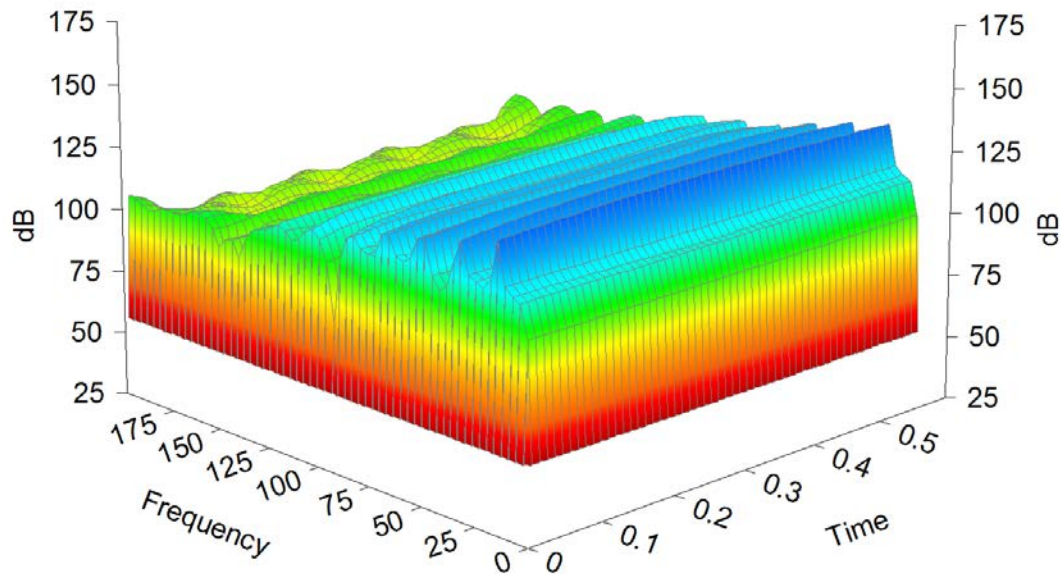


**Figure 7: Sound pressure level for engine normal function**

**Table 5: Average and maximum sound pressure level**

	Engine normal function	Deactivated cylinder	Active cylinder
Maximum sound pressure level [dB]	110	115	115
Average sound pressure level [dB]	92	86	86

## 5. Conclusions

The paper presents a bi-physics (tribo-dynamics) approach to the design analysis of elliptic bore big end bearings of internal combustion engines. The analysis combines inertial piston-connecting rod-crank dynamics and bearing dynamic stability with mixed elasto-hydrodynamics of bearing conjunction, a controlled volume thermal balance model and acoustic emission. This approach combines fuel efficiency and NVH refinement which are the key drivers in modern engine development. The influence of cylinder deactivation system pursued in modern engine development for low speed light load driving conditions upon bearing performance is also ascertained. The holistic and integrative approach to big end bearing dynamics has not hitherto reported in literature. The analysis shows that CDA makes marginal differences in parasitic frictional losses in engine bearing performance and any significant gain would depend on the brake specific fuel consumption. The same may be more significant in piston-cylinder conjunctions. It is shown that sufficient swept volume with retained residual exhaust gas charge within the deactivated cylinders can ensure bearing whirl stability. It is shown that cylinders in partially deactivated engine configuration exhibit

a lower average steady noise emission, but with a higher degree of transient content. This suggests a greater contribution to engine rumble with deactivated cylinders.

## References

- [1]- Tung, S.C. and McMillan, M.L., "Automotive tribology overview of current advances and challenges for the future", *Tribology International*, 37 (7), 2004, pp. 517-536
- [2]- Falkowski, A., McElwee, M., and Bonne, M., "Design and Development of the DaimlerChrysler 5.7L HEMI® Engine Multi-Displacement Cylinder Deactivation System," SAE Technical Paper 2004 01-2106, 2004, doi: 10.4271/2004-01-2106.
- [3]- Roberts, C., "Variable Valve Timing," SwRI Project No. 03.03271, Clean Diesel III Program, March 2004.
- [4]- Wilcutts, M., Switkes, J., Shost, M., and Tripathi, A., "Design and Benefits of Dynamic Skip Fire Strategies for Cylinder Deactivated Engines," *SAE Int., J. Engines* 6(1), 2013, pp. 278-288, 2013, doi:10.4271/2013-01-0359.
- [5]- Rahnejat, H., *Multi-body Dynamics: Vehicles, Machines and Mechanisms*, Joint publishers: Professional Engineering Publishing (UK) and SAE (USA), 1998, ISBN: 0-7680-0269-9
- [6]- Senapati, U., McDevitt, I., and Hankinson, A., "Vehicle Refinement Challenges for a Large Displacement Engine with Cylinder Deactivation Capability," SAE Technical Paper 2011-01-1678, 2011, doi:10.4271/2011-01-1678.
- [7]- Tangasawi, O., Theodossiades, S. and Rahnejat, H., "Lightly loaded lubricated impacts: Idle gear rattle", *J. Sound and Vibration*, 308(3), 2007, pp. 418-430
- [8]- Kushwaha, M., Gupta, S., Kelly, P. and Rahnejat, H., "Elasto-multi-body dynamics of a multicylinder internal combustion engine", *Proc. Instn. Mech. Engrs., Part K: J. Multi-body Dynamics*, 216(4), 2002, pp. 281-293
- [9]- Menday, M.T., Rahnejat, H. and Ebrahimi, M., "Clonk: an onomatopoeic response in torsional impact of automotive drivelines", *Proc. Instn. Mech. Engrs., Part D: J. Automobile Engng.*, 213(4), 1999, pp. 349-357
- [10]- Gohar, R. and Rahnejat, H., *Fundamentals of Tribology*, Imperial College Press, London, 2008, ISBN-13 978-1-84816-184-9
- [11]- Mishra, P.C. and Rahnejat, H., "Tribology of big end bearings" in Rahnejat, H (Ed.), *Tribology and dynamics of engine and power train*, Woodhead Publishing, Cambridge, UK, 2010 ISBN: 978-1-84569-361-9
- [12]- Bates, T. W., Fantino, B., Launay, L., Frêne, J., "Oil film thickness in an elastic connecting-rod bearing: comparison between theory and experiment", *Tribology Transactions* 33(2), 1990: pp. 254-266.
- [13]- Conway-Jones, J. M., F. A. Martin, and R. Gojon. "Refinement of engine bearing design techniques", *Tribology International*, 24 (2), 1991, pp. 119-127

- [14]- Aitken, M. B., and H. McCallion. "Elastohydrodynamic Lubrication of Big-End Bearings Part 1: Theory", Proc. Instn. Mech. Engrs., Part C: J. Mechanical Engineering Science 205(2), 1991, pp. 99-106.
- [15]- Aitken, M. B., and H. McCallion. "Elastohydrodynamic Lubrication of Big-End Bearings Part 2: Ratification", Proc. Instn. Mech. Engrs., Part C: J. Mechanical Engineering Science 205(2), 1991, pp. 107-119
- [16]- Balakrishnan, S., McMinn, C., Baker, C.E. and Rahnejat, H., "Fundamentals of crank and camshaft support journal bearings", in Rahnejat, H. (Ed.), Tribology and dynamics of engine and powertrain, Woodhead Publishing, Cambridge, UK, 2010, ISBN: 978-1-84569-361-9
- [17]- Boedo, S., and Booker, J. F., "Finite element analysis of elastic engine bearing lubrication: Application", Revue Européenne des Eléments Finis, 10, 2001, pp. 725-740
- [18]- Bonneau, D., Guines, D., Frene, J. and Toplosky, J., "EHD analysis, including structural inertia effects and a mass-conserving cavitation model" Trans. ASME, J. Tribology, 117(3), 1995, pp. 540-547.
- [19]- Rahnejat, H., "Multi-body dynamics: historical evolution and application", Proc. Instn. Mech. Engrs., Part C: J. Mechanical Engineering. Science, 214(1), 2000, pp. 149-173
- [20]- Majumdar, B.C., "The effect of roughness parameter on the performance of hydrodynamic journal bearings with rough surfaces", Tribology International, 32, 1999, pp. 231-236
- [21]- Kim, B-J. and Kim, K-W., "Thermo-elastohydrodynamic analysis of connecting rod bearing in internal combustion engine." Trans. ASME, J. Tribology, 123(3), 2001, pp. 444-454
- [22]- Stefani, F. A. and Reborn, A.U., "Finite element analysis of dynamically loaded journal bearings: influence of the bolt preload", Trans. ASME, J. Tribology, 124(3), 2002, pp. 486-493
- [23]- Crosby, W.A., "Thermal considerations in the solution of finite journal bearings", Wear, 64, 1980, pp.15-32
- [24]- Boncompain R., Fillon, M. and Frene, J., "Analysis of thermal effects in hydrodynamic bearings", Trans. ASME, J. Tribology, 108, 1986, pp. 219-224
- [25]- Thomson, W. T., Vibration Theory and Applications, 5<sup>th</sup> Impression, Prentice Hall Inc., Guildford, Surrey, UK, 1976, ISBN-0-04-531003-3

- [26]- Greenwood, J. A. and Tripp, J. H., “The contact of two nominally flat rough surfaces”, Proc. Instn. Mech. Engrs, 185, 1970-71, pp. 625-633
- [27]- Teodorescu, M., Balakrishnan, S. and Rahnejat, H., “Integrated tribological analysis within a multi-physics approach to system dynamics”, Tribology and Interface Engineering Series (Elsevier), 48, 2005, pp.725-737
- [28]- Mohammadpour, M., Theodossiades, S. and Rahnejat, H., “Elastohydrodynamic Lubrication of hypoid gears at high load”, Proc. Instn. Mech. Engrs., Part J: J. Engineering Tribology, 226 (3), 2012, pp. 183-198
- [29]- Elrod, H. G., : A cavitation algorithm. Trans. ASME, J. lubn. Tech. 103 (3), 350-354 (1981)
- [30]- Morris, N., Rahmani, R., Rahnejat, H., King, P.D. and Fitzsimons, B., “Tribology of piston compression ring conjunction under transient thermal mixed regime of lubrication”, Tribology Int., 59, 2013, pp. 248-258
- [31]- Shigley, J. E. and Uicker Jr, J. J., Theory of machines and mechanisms, McGraw-Hill, 1995, New York, ISBN 0070569304
- [32]-Suryanarayana, N.V.,”Forced convection internal flows”, pp. 3-47–55 in: Kreith, F, (Ed.) The Handbook of Thermal Engineering, CRCPress, 2000, USA
- [33]- Carslaw H.S. and Jaeger J.C., Conduction of heat in solids, 2nd ed. Oxford: Science Publications, 2005, Oxford, UK
- [34] Chong, W.W.F., Teodorescu, M. and Rahnejat, H., “Nanoscale elastoplastic adhesion of wet asperities”, Proc. Instn. Mech. Engrs., Part J: J. Engineering Tribology, 2013, doi: 10.1177/1350650112472142
- [35]- Briscoe, B. J. and Evans, D. C. B., “The shear properties of Langmuir-Blodgett layers”, Proc. Roy. Soc., Series A: Mathematical and Physical Sciences, 380(1779), 1982, pp. 389-407.
- [36]- Rho, B-H and Kim, K-W, “Acoustical properties of hydrodynamic journal bearings”, Tribology Int., 36, 2003, pp. 62-66
- [37]- Leventhall, H. G., "Low frequency noise and annoyance.", Noise and Health, 6(23), 2004, pp. 59-72